Supplementary Information

A modular switch for spatial Ca^{2+} selectivity in the calmodulin regulation of Ca_V channels

Dick *et al* (submitted) *Nature* — 2207-07-06990D

1. Additional data for Fig. 1

1.1. N-lobe dominance of CDI within the cBBBBb channel chimera

Is the strong CDI of chimeric cBBBBb Ca^{2+} channels (Fig. S1a) still selectively mediated by Ca^{2+} binding to the N-lobe of CaM? Previously this has been demonstrated for the full-length $Ca_V2.2$, from which cBBBBb has been derived[2]. To test for such selectivity, we utilized mutant CaM constructs in which the Ca^{2+} binding ability of one or both lobes is abrogated. Co-expression of cBBBBb and a mutant CaM which entirely lacks a functional Ca^{2+} binding site (CaM_{1234}) virtually eliminated CDI under high buffer conditions (Fig. S1b). This indicates that such regulation remains under the control of CaM. We further probed the lobe specificity of the chimera by co-expression with either a C-lobe sparing mutant (CaM_{12}) or an N-lobe sparing version (CaM_{34}). The resulting currents demonstrated strong suppression of calcium regulation under C-lobe only conditions (Fig. S1c), while selective functionality of the N-lobe sufficed to promote strong CDI. (Fig. S1d) Thus, the change in the spatial Ca^{2+} selectivity imparted by the amino terminus of α_{1C} still pertains to an N-lobe mediated process

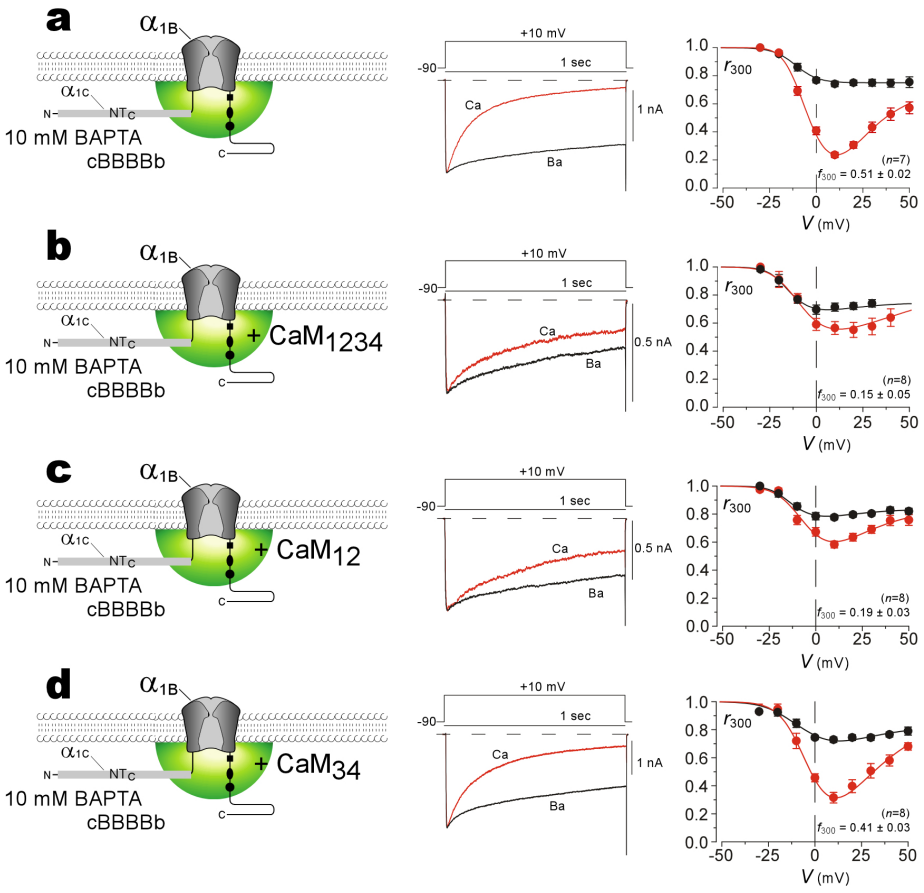

Fig. S1 Left column cartoons the cBBBBb channel α_1 subunit, and the corresponding recombinant CaM expressed in the specific experiment. Middle panels display exemplar traces in Ca^{2+} (red) and Ba^{2+} (black) at 10 mV. Right displays the fraction of peak current remaining after 300 ms of depolarization; shown is the average ± SEM across multiple cells. **a,** Chimeric channel cBBBBb exhibits strong CDI even under high 10 mM BAPTA Ca^{2+} buffering (local signal). Reproduced from Fig. 1c of main text, for reference. **b**, CaM_{1234} all but eliminates CDI of cBBBBb in high buffering. **c**, CaM_{12}, which isolates C-lobe signaling, severely diminishes CDI on par with CaM_{1234}. **d**, CaM_{34}, which isolates N-lobe signaling, spares the potent CDI of cBBBBb in 10 mM BAPTA.

1.2. Further FRET two-hybrid results for Figs. 1e-g

Binding of various amino-terminal $Ca_V2.2$ and $Ca_V1.2$ fragments to CaM were assayed by means of FRET two-hybrid experiments[3]. The table below lists the full set of parameter values for experiments corresponding to Figs 1d-f of the main text. We also show several exemplar binding curves (Fig. S2).

FRET Partner	Construct Name	Construct Source	aa range	mean FR	SEM	Ncell	KdEFF x 1000	FRmax
apoCaM	NT-B	alpha 1B	1-95	0.8336014	0.07114	4	>10,000	9.4
Ca2+/CaM	NT-B	alpha 1B	1-95	1.0238678	0.02738	14	>10,000	9.4
apoCaM	NT-C	alpha 1C	1-158	0.84752	0.02209	5	>10,000	9.4
Ca2+/CaM	NT-C	alpha 1C	1-158	1.9823281	0.06684	34	23	3.4
apoCaM	NT-C1	alpha 1C	1-66	0.8795097	0.0413	5	>10,000	9.4
Ca2+/CaM	NT-C1	alpha 1C	1-66	0.8229601	0.05374	5	>10,000	9.4
apoCaM	NT-C3	alpha 1C	132-158	0.8939995	0.01078	9	>10,000	9.4
Ca2+/CaM	NT-C3	alpha 1C	132-158	0.8818507	0.0572	9	>10,000	9.4
apoCaM	NT-C2	alpha 1C	67-131	0.8476489	0.0427	27	>10,000	9.4
Ca2+/CaM	NT-C2	alpha 1C	67-131	2.2481183	0.27816	16	20	3.2
Ca2+/CaM	NT-C67a	alpha 1C	67-116	6.2920489	0.31761	11	16	7.4
Ca2+/CaM	NT-C67b	alpha 1C	67-98	4.9808518	0.31317	17	20	6.6
Ca2+/CaM	NT-C78a	alpha 1C	78-131	5.4167041	0.75787	8	11	7.6
Ca2+/CaM	NT-C78b	alpha 1C	78-116	5.5006324	0.31551	25	15	7.9
Ca2+/CaM	NT-C78c	alpha 1C	78-98	1.7662346	0.10561	20	12	2.2
Ca2+/CaM	NT-C82	alpha 1C	82-116	5.4232958	0.55117	10	14	7.1
Ca2+/CaM	NT-C83	alpha 1C	83-116	1.2292352	0.2949	9	6390	9.4
Ca2+/CaM	NT-C85	alpha 1C	85-116	1.1814872	0.14936	5	6384	9.4
Ca2+/CaM	NT-C88a	alpha 1C	88-131	0.6384994	0.07663	25	>10,000	9.4
Ca2+/CaM	NT-C88b	alpha 1C	88-98	0.5665696	0.06456	22	>10,000	9.4
Ca2+/CaM	NT-C W82A	alpha 1C	78-116	0.943533	0.10761	34	>10,000	9.4

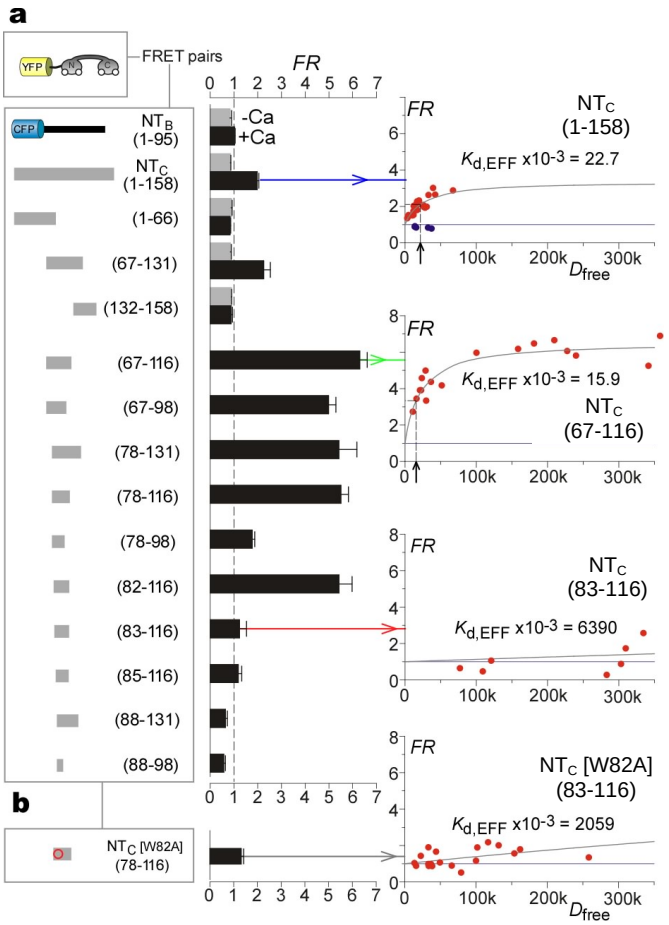

Fig. S2 A novel CaM binding site is localized within the amino terminus of α_{1C}. **a,** FRET analysis was performed on YFP tagged CaM pitted against various CFP tagged segments of the α_{1C} amino-terminus (NT_C), as well as the amino-terminus of α_{1B} (NT_B). A binding curve fit to the raw FRET ratios (right) was used to calculate $K_{d,EFF}$. Red indicates data obtained in saturating Ca^{2+}, while blue corresponds to Ca^{2+}-free CaM. While NT_B exhibited no binding to CaM (top row), full length NT_C bound CaM in a Ca^{2+}-dependent manner (second row). Sucessive deletions demonstrated an abrupt loss of binding with the removal of the tryptophan at NT_C 82. **b**, Mutation of the key W82 within NT_C also eliminates FRET binding.

2. Additional data for Fig. 2

2.1. Detailed mapping of key amino acid residues in *NSCaTE*

Electrophysiological data demonstrate that 3 amino-acid residues are particularly important for the induction of strong, locally mediated CDI in the chimeric cBBBBb construct (Figs. 2 c,d main text, Fig. S3a). Mutating these residues to alanines reduced CDI (in high buffering) with the rank order W82A > I86A > R90A. For optimal comparison of these N-lobe mediated CDI effects with binding, we examined NT_C peptide interactions with a mutant CaM_{34}, wherein Ca^{2+} binding is restricted to the N-lobe[4,5]. Accordingly, FRET assays paired EYFP–CaM_{34} with ECFP–tagged NT_C peptides containing corresponding point mutations. The resulting binding curves indicated variable attenuation of Ca^{2+}/CaM_{34} interaction with the different mutations, compared to the wildtype NT_C-(78-116) (Fig. S3b). This attenuation showed the same rank order as CDI effects (Fig. 2d of main text).

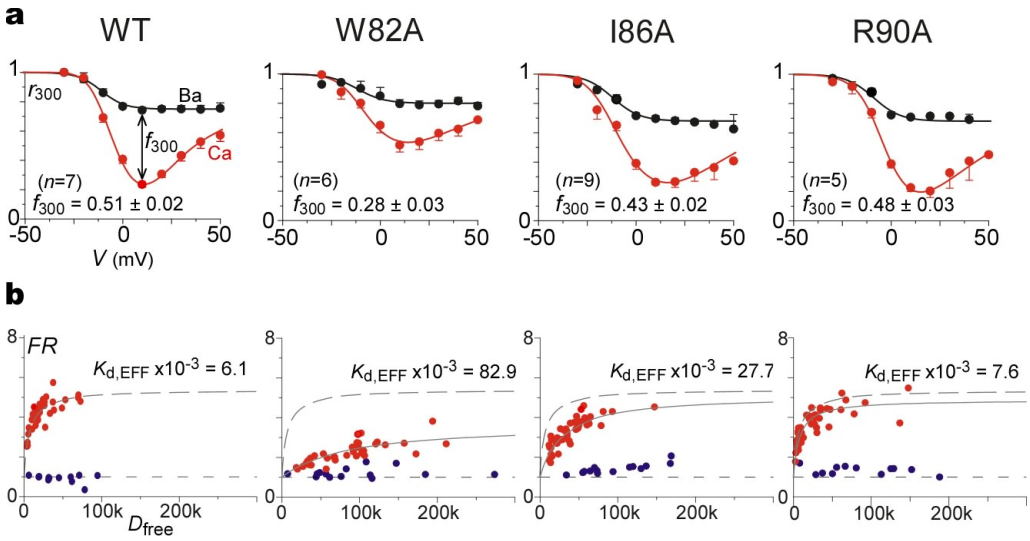

Fig. S3 Identification of three key amino acids within *NSCaTE*. **a**. Population averages for CDI of Δ78cBBBBb channels with point mutations indicated at top in high buffering. The fraction of peak current remaining after 300 ms of depolarization is shown as the average ± SEM across multiple cells. **b,** FRET two-hybrid assays, testing YFP–CaM_{34} against CFP–NT_C-(78-116) constructs with corresponding point mutations. Red indicates binding to Ca^{2+}/CaM, blue indicates the lack of binding to apoCaM. Dotted curve indicates the wild-type binding curve in Ca^{2+}. Format as in Fig. 1e (right) of main text.

3. Additional data for Fig. 3

3.1. The *NSCaTE* within NT_D has analogous properties to NT_C.

Fig. 3b of the main text demonstrates CaM binding to NT_D. Mutation of the tryptophan to alanine (W44A) in this $Ca_V1.3$ *NSCaTE* eliminates Ca^{2+}/CaM binding by FRET (Fig. S4a). NT_D is also capable of inducing CDI under local buffering conditions in a dBBBBb chimeric channel, as shown by the population data in Fig. S4b.

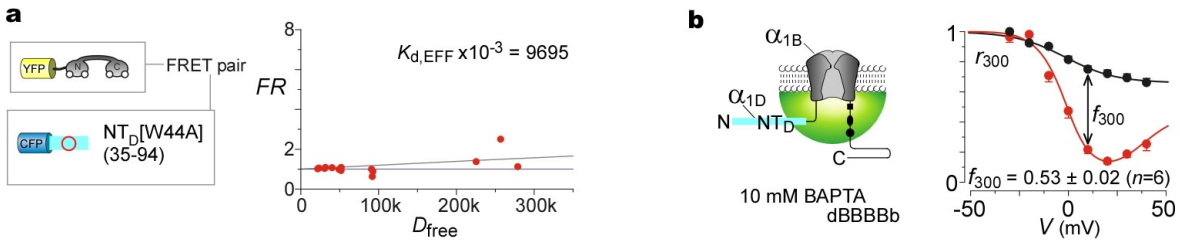

Fig. S4 *NSCaTE* functions within NT_D. **a**, FRET binding between NT_D and Ca^{2+}/CaM is eliminated by a single amino acid mutation. FRET two-hybrid assays pitting YFP–CaM against an amino terminal segment of $Ca_V1.3$ spanning amino acids 35-94 and containing a W44A mutation. Binding curve pertains to elevated Ca^{2+}, and the format is as in Fig. 1e of the main text. **b**, Replacement of the amino terminus of $Ca_V2.2$ with that of $Ca_V1.3$ (creating the chimera dBBBBb) produces strong CDI in 10 mM BAPTA. Population data correspond to exemplar traces in Fig. 3c of the main text. Format as in Fig. 1a (right) of the main text.

3.2. Amino terminal deletion in $Ca_V1.3$ abolishes N-lobe CDI under strong buffering

The presence of *NSCaTE* in the amino terminus of native $Ca_V1.3$ channels enables N-lobe CaM-mediated regulation responsive to local Ca^{2+} signals (Fig. 3d main text, Fig. S5a). Removal of a portion of the amino terminus (including the critical W44 within *NSCaTE*) transforms N-lobe signaling to a global preference within these channels (Figs. S5 b,c)

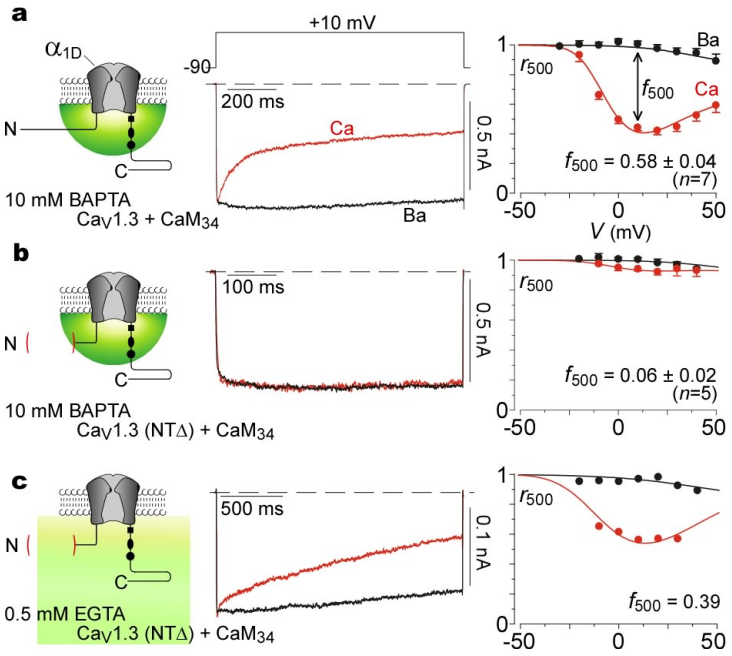

Fig. S5 *NSCaTE* functions in native $Ca_V1.3$ channels, producing N-lobe CaM-mediated CDI under local buffering conditions. **a,** Strong CDI of $Ca_V1.3$ in high buffering reproduced from Fig. 3d of main text for reference, using 500-ms metrics. **b,** Deletion of the first 44 amino acids of $Ca_V1.3$ eliminates this CDI. **c,** Low buffering conditions reveal the presence of globally responsive CDI in this deletion construct.

3.3. CaM_{1234} eliminates $Ca_V1.3$ CDI under 0.5 mM internal EGTA buffering

As demonstrated in Fig. 3d of the main text, $Ca_V1.3$ exhibits strong N-lobe CDI under high buffering conditions, as predicted for a channel possessing an inherent *NSCaTE*. In demonstrating the effect of mutations disrupting this *NSCaTE* motif, we suggested that these mutations simply altered the spatial Ca^{2+} selectivity of N-lobe CDI, rather than altogether eliminating this process. In fact, CDI of the mutant channel re-emerges in low (0.5 mM EGTA) Ca^{2+} buffering. To confirm that the resurfacing of CDI in low buffering reflects a genuinely CaM-mediated process, and not another form of inactivation, we here confirm that coexpressing CaM_{1234} with $Ca_V1.3$ completely eliminates CDI under low (0.5 mM EGTA) buffering conditions. Previously, we showed this same effect under moderate 5 mM EGTA conditions[6].

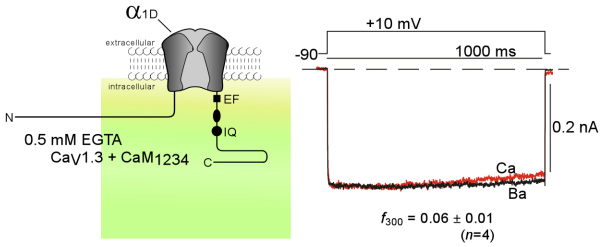

Fig. S6 Left, cartoon of the $Ca_V1.3$ channel coexpressed with CaM_{1234} under low buffering conditions (0.5 mM EGTA internal). Right, exemplar Ca^{2+} (red) and Ba^{2+} (black) traces at 10 mV in the presence of 0.5 mM EGTA. The average f_{300} value is given as mean ± SEM. Current bar for Ca^{2+}.

3.4. Amino terminal deletion in $Ca_V1.2$ abolishes N-lobe CDI under strong buffering

NSCaTE within the amino terminus of native $Ca_V1.2$ channels enables N-lobe CaM-mediated regulation responsive to local Ca^{2+} signals (Fig. 3e main text, Fig. S7a). Removal of the entire amino terminus transforms N-lobe signaling to a global preference within these channels.

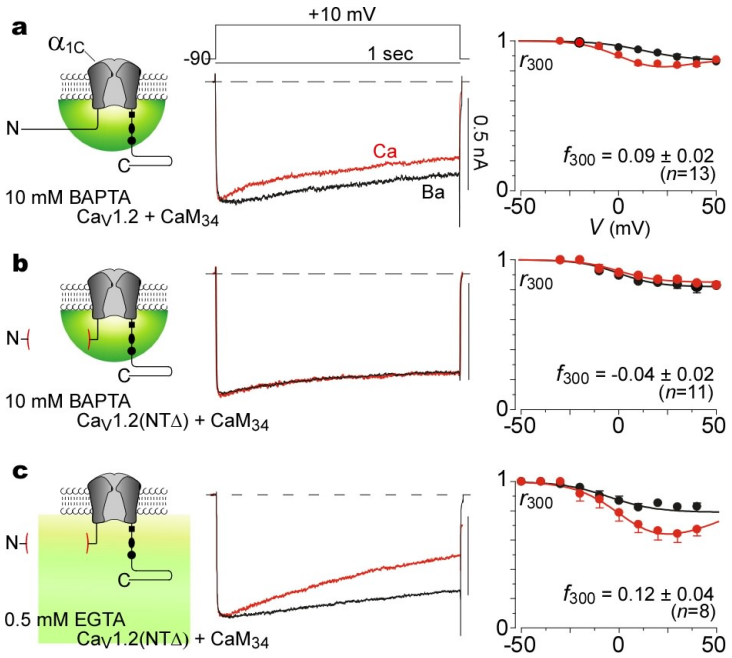

Fig. S7 *NSCaTE* is functional within native $Ca_V1.2$ channels, yielding N-lobe CaM mediated CDI that persists under local Ca^{2+} buffering conditions. **a**, Strong CDI of $Ca_V1.2$ in high buffering reproduced from Fig. 3e of main text for reference. **b,** Deletion of the first 142 amino acids of $Ca_V1.2$ eliminates this CDI. **c**, Low buffering conditions reveal the presence of globally responsive CDI in the deletion construct. **a-c,** The average f_{300} values are given as mean ± SEM. Current bars for Ca^{2+}.

3.5. CaM_{1234} eliminates $Ca_V1.2$ CDI under 0.5 mM internal EGTA buffering

By analogy to the control experiment done for $Ca_V1.3$ (section 3.3), we also demonstrate that the CDI of $Ca_V1.2$ channels in physiological buffering conditions (0.5 mM EGTA) is mediated entirely by CaM.

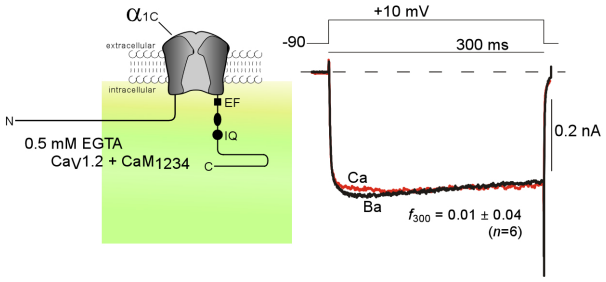

Fig. S8 Left, cartoon of the $Ca_V1.2$ channel coexpressed with CaM_{1234} under low buffering conditions (0.5 mM EGTA internal). Right, exemplar Ca^{2+} (red) and Ba^{2+} (black) traces at 10 mV in the presence of 0.5 mM EGTA. The average f_{300} value is given as mean ± SEM.

4. Prokaryotic *NSCaTE*

4.1. Bioinformatic strategies for *NSCaTE* phylogenetic contexts

Sequence alignments were generated using ClustalW with a gap open penalty of 10, a gap extension penalty of 0.5, and free end gaps. Channel amino terminal sequences (Fig. 3a, Fig. S9) were aligned for the length of the amino terminus until the start of the S1 region of each channel, and were subsequently cropped for display. Alignments for dendrogram construction (Fig. 4a) were based upon entire channel protein sequences. Subsequent dendrogram construction was done according to a Jukes-Cantor Neighbor-Joining method using the *Xanthomonas campestris* TonB dependent receptor as an outgroup. Prediction of the alpha helix within the amino-termini of $\alpha_{1C/D}$ was done utilizing the web based nnpredict utility[7].

Accession numbers for channel sequences used in the phylogenic analysis are as follows:
α1G human: O43497 α1I mouse: NP_001037773.1 T-type *C. elegans*: AAP79881.1 α1A mouse: P97445 α1A human: O00555 α1B mouse: O55017, α1B human: Q00975, α1E mouse: NP_033912.2, α1E human: Q15878 non-L type *C. elegans*: 2110386A, non L-type squid: BAA13136.2, L-type coral: AAD11470.1, L-type jellyfish: AAC63050.1, α1C mouse: Q01815, α1C rat: AAL47073, α1C rabbit: P15381, α1C human: NP_000710.5, α1C zebra fish: NP_571975.1 α1D rat: NP_058994, α1D mouse: BAC77259.1, α1D human: NP_000711.1, α1D hampster: Q99244, α1D chicken: AAC08304.1, α1Da zebra fish: NP_982351.1, α1Db zebra fish: AAS20587.1, α1F mouse: Q9JIS7, α1F rat: NP_446153.1, α1F human: O60840, α1S human: Q13698, α1S rat: Q02485, α1S zebra fish: NP_999891.1, L-type tunicate: BAA34927, L-type *Drosophila*: NP_723953.1, L-type *C. elegans*: AAC47755.1, *X. campestris pv. campestris* TBDR: NP_637920.1, *X. campestris pv vesicatoria* TBDR: YP_364625.1, *X. axonopodis pv. citri*: TBDR: NP_643051.1. LCa_V1a *Lymnaea*: AA083838.2, LCa_V1b *Lymnaea: AA083839.1,* LCa_V2 a *Lymnaea: AA083841.1,* LCa_V2b *Lymnaea: AA083842.1.*

Blast searches were done on the NCBI BLASTp server using WQAAIDAARQAKLMGSA as a search sequence. Iterative PHI BLAST searches were also done using the PHI pattern WxxxIxxxR, however few new relevant hits were obtained. CaM-like proteins in *Xanthomonas* were found by doing repeated protein and nucleotide blast searches for known EF-hand motifs[8]. Using the EF-hand motif from calsymin (AAG21376.1), a known CaM-like protein in *Rhizobium etli* bacteria[8,9], we were able to identify two EF-hand containing proteins in *Xanthomonas*. Additional protein and nucleotide BLAST searches using these two hits as a template revealed five EF-hand containing proteins in each of the three *Xanthomonas* organisms possessing the *NSCaTE* motif. Of these, one protein was highly conserved across the three strains and demonstrated four EF-hand motifs, and a 47% homology with the CaM from the amoeba *Dictyostelium discoideum*. (XP_641695.1) Accession numbers for the CaM-like protein candidates are: *X. campestris pv. campetris*, NP_636517.1; *X. campestris pv vesicatoria*, YP_363005.1; and *X. axonopodis pv. citri*, NP_641576.1. Alignment of these proteins was done with ClustalW as before, with additional manual alignment of EF-hand motifs.

4.2. Alignment of amino termini from L-type channels

NSCaTE is found in $Ca_V1.2/1.3$ of advanced species, but is absent in lower species which do not have differentiated L-type channel sub isoforms. Extensive blast searches (Supplementary Information 4.1) reveal a lack of *NSCaTE* motifs in lower species until bacteria, where several organisms contain regions bearing high homology with *NSCaTE*, particularly at the 3 critical residues described in the main text of this paper. To probe the potential function of such prokaryotic *NSCaTE* motifs, we focus on the *NSCaTE* found in *Xanthomonas*, a pathogen of cruciferous plants.

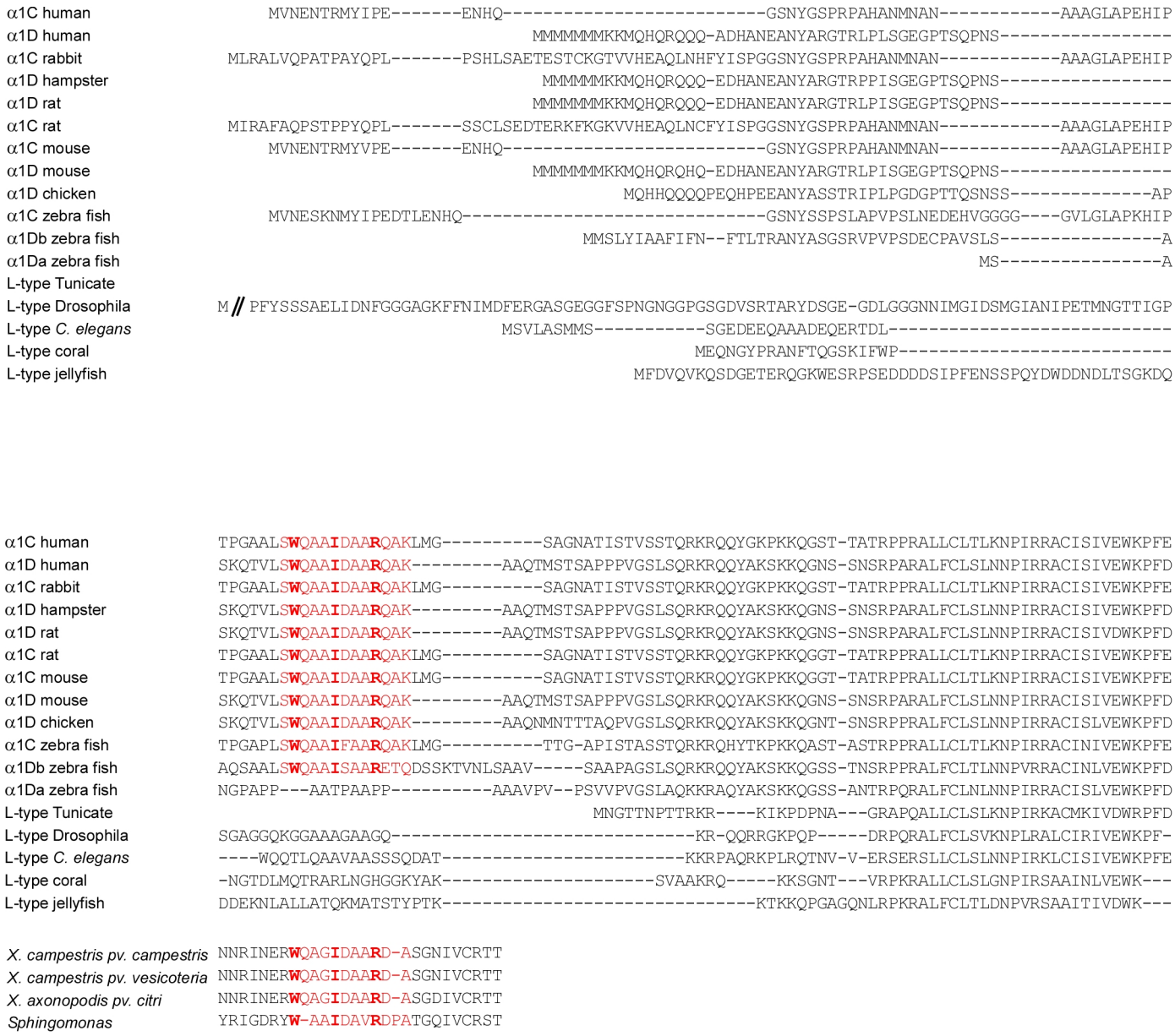

Fig. S9 Sequence alignment showing *NSCaTE* (red) within amino termini of certain Ca_V1 channels, and within lower organisms such as the Ton B dependent receptor (bottom set, bottom 4 rows).

4.3. Prokaryotic *NSCaTE* interacts with Ca^{2+}/CaM

Fitting with a functional role for prokaryotic *NSCaTE* , FRET assays show that Ca^{2+}/CaM (but not apoCaM) binds to the Ton B Dependent Receptor *NSCaTE* motif.

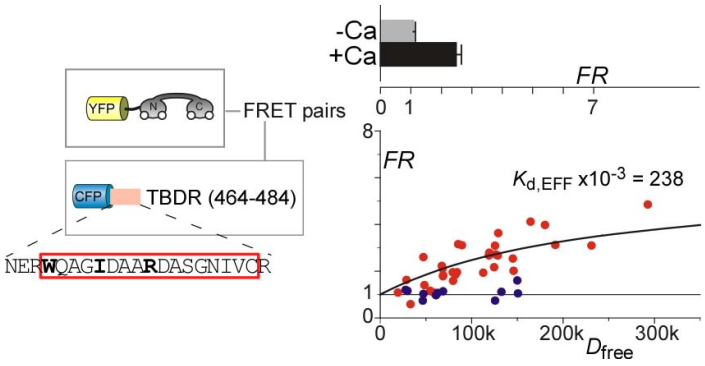

Fig. S10 FRET two-hybrid assays confirming Ca^{2+}/CaM(red), but not apo CaM (Blue) interaction with bacterial *NSCaTE* . Format as in Fig. 1e of the main text.

4.4. CaM-like molecules in *Xanthomonas*

Though CaM itself is absent in bacteria, CaM-like proteins have been identified in some bacteria[8]. Motivated by the discovery of *NSCaTE* in TonB dependent receptors of three *Xanthomonas* bacteria, we searched the NCBI protein and genomic databases (http://www.ncbi.nlm.nih.gov/BLAST/) for EF-hand-containing proteins from these bacteria. Our results indicated at least 5 such proteins within each of the organisms. Here we display one result which was highly conserved across these bacteria, and bears a good resemblance to CaM, providing a possible endogeneous partner for the prokaryotic *NSCaTE*.

```
Dictyostelium discoideum (CaM)   MASQESL-----------------------------------------------TEEQIA
X. campestris pv. vesicotoria    MTSRKPFLALAVLAALSAGTAFAATVPAPGDAPRPAKLDKNGDGVIDRSEAAADP-----
X. axonopodis pv citri           MTSRKPFLALAVLAALSTGTAFAATVPAPGDAPRPAKLDKNGDGVIDRSEAAADP-----
X. campestris pv. campestris     MTSRKPFLALAVLAALSTASAFAATPPAAGDAPRPAKLDTNGDGVIDRSEAAADP-----

                                 En--nn--n*-*-*G-I*--*n--nn--n        En--nn--n*-*-*G-I*--*n--nn--n
Dictyostelium discoideum (CaM)   EFKEAFSLFDKDGDGSITTKELGTVMRSLGQNPTEAELQDMINEVDADGNGNIDFPEFLTMMARKMQDTDTEE
X. campestris pv. vesicotoria    TLAAQFDTLDTNKDGKLSRDERPHHRGP-----GRGGRGEWMAKLDTNKDGRISREEAKADPK----------
X. axonopodis pv citri           TLAAQFDTLDTNKDGKLSRDERPHHRGPGRD--GRGGRGEWMAKLDTNKDGRISREEAKADPK----------
X. campestris pv. campestris     RLAAKFDSLDTNKDGKLSRDERPHRRGPGR-----DGRGEMWAKLDANKDGRISRDEAKADPK----------

                                 En--nn--n*-*-*G-I*--*n--nn--n        En--nn--n*-*-*G-I*--*n--nn--n
Dictyostelium discoideum (CaM)   EIREAFKVFDKDGNGYISAAELRHVMTSLGEKLTNEEVDEMIREADLDGDGQVNYDEFVKMMIVRN-------
X. campestris pv. vesicotoria    -FAARFDQMDLNKDGFVDRADRELRMQQH--------RDAWFAKADTDKDGKLSKAEFDAASKWRGGHGPGG-
X. axonopodis pv citri           -FAARFDQMDLNKDGFVDRADRELRMQQH--------RDAWFAKADTDKDGKLSKAEFDAASKWRGGHGPGG-
X. campestris pv. campestris     -FAARFDQMDINKDGFVDRADREQRMQQH--------RDAWFAKADTDKDGKLSKAEFDAASKLRGEHGPRGE

                                 --------------------
Dictyostelium discoideum (CaM)
X. campestris pv. vesicotoria    MGRHGDDGKPAPASAPAANR
X. axonopodis pv citri           MGRHGDDGKPSPATAPATNR
X. campestris pv. campestris     HGERGEHGKRPMPAKPAAGN
```

Fig. S11 Alignment of CaM from *Dictyostelium* with three CaM-like molecules present in genomic sequence from *Xanthamonas* (see section 3.2 for sequence details). The four EF-hand motifs of CaM[1] are clearly present in the bacterial molecules. The standard EF-hand motif pattern is displayed above each such module in CaM. n, hydrophobic residues; *, oxygen-bearing residue; E,G,I, highly conserved charged and hydrophobic anchors. Note that the central 'G' is present in all molecules.

5. References

1. Babitch, J. Channel hands. *Nature* **346**, 321-2 (1990).
2. Liang, H. et al. Unified mechanisms of Ca2+ regulation across the Ca2+ channel family. *Neuron* **39**, 951-60 (2003).
3. Erickson, M. G., Liang, H., Mori, M. X. & Yue, D. T. FRET two-hybrid mapping reveals function and location of L-type Ca^{2+} channel CaM preassociation. *Neuron* **39**, 97-107 (2003).
4. DeMaria, C. D., Soong, T. W., Alseikhan, B. A., Alvania, R. S. & Yue, D. T. Calmodulin bifurcates the local Ca2+ signal that modulates P/Q-type Ca2+ channels. *Nature* **411**, 484-9 (2001).
5. Peterson, B. Z., DeMaria, C. D., Adelman, J. P. & Yue, D. T. Calmodulin is the Ca2+ sensor for Ca2+ -dependent inactivation of L-type calcium channels. *Neuron* **22**, 549-58 (1999).
6. Yang, P. S. et al. Switching of Ca2+-dependent inactivation of Ca(v)1.3 channels by calcium binding proteins of auditory hair cells. *J Neurosci* **26**, 10677-89 (2006).
7. Kneller, D. G., Cohen, F. E. & Langridge, R. Improvements in protein secondary structure prediction by an enhanced neural network. *J Mol Biol* **214**, 171-82 (1990).
8. Michiels, J., Xi, C., Verhaert, J. & Vanderleyden, J. The functions of Ca(2+) in bacteria: a role for EF-hand proteins? *Trends Microbiol* **10**, 87-93 (2002).
9. Xi, C., Schoeters, E., Vanderleyden, J. & Michiels, J. Symbiosis-specific expression of Rhizobium etli casA encoding a secreted calmodulin-related protein. *Proc Natl Acad Sci U S A* **97**, 11114-9 (2000).